ACS Catalysis
Research Article
pubs.acs.org/acscatalysis

NIR-Responsive Photocatalytic Activity and Mechanism of $NaYF_4$:Yb,Tm@TiO_2 Core–Shell Nanoparticles

Yanna Tang, Weihua Di,* Xuesong Zhai, Renyuan Yang, and Weiping Qin*

State Key Laboratory on Integrated Optoelectronics, College of Electronic Science and Engineering, Jilin University, Changchun 130012, PR China

Ⓢ *Supporting Information*

ABSTRACT: Core–shell structured nanoparticles for near-infrared (NIR) photocatalysis were synthesized by a two-step wet-chemical route. The core is composed of upconversion luminescence $NaYF_4$:Yb,Tm prepared by a solvothermal process, and the shell is anatase TiO_2 nanocrystals around $NaYF_4$ particles formed via a method similar to a Stöber process. Methylene blue compound as a model pollutant was used to investigate the photocatalytic activity of $NaYF_4$:Yb,Tm@TiO_2 composites under NIR irradiation. To understand the nature of NIR-responsive photocatalysis of $NaYF_4$:Yb,Tm@TiO_2, we investigated the energy transfer process between $NaYF_4$:Yb,Tm and TiO_2 and the origin of the degradation of organic pollutants under NIR radiation. Results indicate that the energy transfer route between $NaYF_4$:Yb,Tm and TiO_2 is an important factor that influences the photocatalytic activity significantly and that the degradation of organic pollutants under NIR irradiation is caused mostly by the oxidation of reactive oxygen species generated in the photocatalytic reaction, rather than by the thermal energy generated by NIR irradiation. The understanding of NIR-responsive photocatalytic mechanism helps to improve the structural design and functionality of this new type of catalytic material.

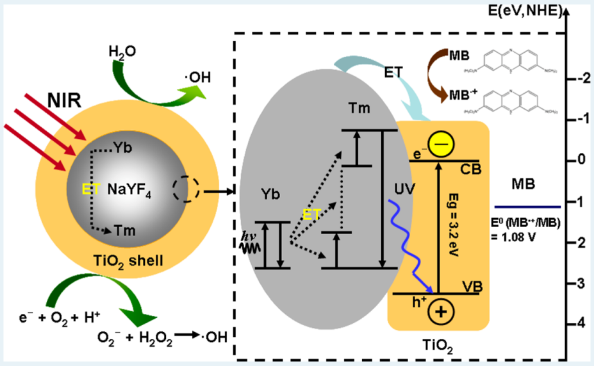

KEYWORDS: *upconversion, TiO_2, photocatalysis, near-infrared, energy transfer*

INTRODUCTION

Air and water pollution is a very serious problem over the world. The application of photocatalysis for pollution treatment has attracted considerable attention in recent years. Since Fujishima and Honda discovered photocatalytic water-splitting on crystalline TiO_2 electrodes for hydrogen production in 1972,[1] research interest in TiO_2 photocatalysis has grown significantly owing to its strong oxidizing power under ultraviolet (UV) light, extraordinary chemical stability, and environmental friendly and biocompatible features;[2−12] however, this photocatalyst requires UV light to be activated because of its large bandgap of ~3.2 eV (for the crystalline anatase phase).[13−15] As we all know, UV light of the solar spectrum occupies only ~5%, whereas the percentages of visible light and near-infrared (NIR) light are about ~49% and ~46%, respectively.[16] Therefore, photons with energy lower than the band gap energy of TiO_2, that is, more than 90% of overall solar spectrum, cannot be utilized to activate this photocatalyst for photocatalysis.

To resolve this problem, much effort has been devoted to extending the absorption of TiO_2 to the visible light region for better use of solar energy. To reach this goal, several strategies have been proposed by adjusting the bandgap toward visible light energies through the introduction of noble metals, cationic substitutions, and anionic doping.[17−27] Although the absorption of TiO_2 by these modification methods could be adjusted to the visible region, the overall catalytic capability was found to decrease due to an increased recombination of photogenerated electrons and holes.[28−30] Therefore, it is still a challenge to find an appropriate way to extend the absorption of TiO_2 to the visible and NIR regions.

The development and advance of nanotechnology opens a new way to obtain functional materials with novel and desirable properties. Because of a large surface-to-volume ratio and easy functionalization of a single nanoparticle, it is easy to construct core–shell heterostructured nanomaterials so as to create novel and complex functionalities through the interaction between the core and the shell.[30−38]

The previous work by our group first demonstrated NIR-driven photocatalysis of broadband semiconductor TiO_2 that was combined with YF_3:Yb,Tm to form a core–shell structure, where YF_3:Yb,Tm acts as a medium for converting NIR to UV and visible light via multiphoton upconversion processes.[16] However, that report did not reveal a NIR photocatalytic mechanism, including the energy transfer process between upconversion luminescence particles and TiO_2 and the actual origin of the organic pollutant degradation. This is the key to understanding the underlying mechanism for further improving

Received: December 13, 2012
Revised: January 22, 2013
Published: January 29, 2013

the functionality of this new type of photocatalytic materials. To address this issue, in this work, a two-step wet-chemical route was used to synthesize core−shell nanoparticles consisting of upconversion luminescence $NaYF_4$:Yb,Tm and an n-type semiconductor TiO_2 for NIR-driven photocatalysis. The reason why YF_3:Yb,Tm in the previous work was replaced by $NaYF_4$:Yb,Tm is that $NaYF_4$ is a more efficient host for upconversion luminescence than YF_3. Steady-state and dynamic fluorescence spectroscopy were applied to demonstrate the energy transfer route between the $NaYF_4$:Yb,Tm and semiconductor TiO_2. The energy transfer route was found to dominate the overall photocatalytic activity. A series of control experiments combined with the detection of reactive oxygen species revealed the actual origin of the degradation of organic pollutants.

■ EXPERIMENTAL SECTION

Preparation of $NaYF_4$:Yb,Tm Nanophosphors. $NaYF_4$:Yb,Tm nanophosphors were prepared by a a solvothermal process using polyvinylpyrrolidone (PVP, K-30) as the chelating agent. All the chemical reagents were used as received without further purification. To obtain rare earth (RE) chlorides, 1 mmol of rare earth oxides Y_2O_3, Yb_2O_3, and Tm_2O_3 with a stoichiometric ratio of 79.5:20:0.5 were dissolved in hydrochloric acid, and then the solution was heated to evaporate the water completely. In a typical synthesis procedure, 1 mmol of RE chlorides with a stoichiometric Y/Yb/Tm ratio of 79.5:20:0.5 was dissolved in 10 mL of ethylene glycol (EG) under vigorous stirring. PVP and NaCl were subsequently added, and the solution was heated to 80 °C to form a homogeneous solution. Another 10 mL of EG containing 4 mmol of NH_4F was added dropwise to the above solution under constant stirring until a transparent solution was formed. The above precursor solution was transferred to a 40 mL autoclave, sealed, and maintained at 180 °C for 12 h. After the autoclave was cooled to room temperature naturally, the product was collected by centrifugation and washed with distilled water and ethanol several times, then dried at 80 °C in air.

Preparation of $NaYF_4$:Yb,Tm@TiO_2 Core−Shell Nanoparticles. Titania-coated $NaYF_4$:Yb,Tm particles were prepared through controlling hydrolysis and condensation of a titanium alkoxide in ethanol.[39] Here, titanium *n*-butoxide ($Ti(OBu)_4$) was employed as the Ti source because the hydrolysis rate of $Ti(OBu)_4$ was ~150 times slower than that of tetraethyl titanate, $Ti(OEt)_4$.[40] A typical procedure for coating titania onto $NaYF_4$:Yb,Tm nanoparticles has been described as follows: $NaYF_4$:Yb,Tm nanoparticles were dispersed in ethanol containing a small trace of Lutensol ON50 aqueous solution. After that, titanium alkoxide dispersed in alcohol was added to the seed particle solution with a controlling speed upon rigorous stirring. The reaction was conducted at room temperature for 20 h. To produce crystalline titania shells, the above precursor solution was transferred to a 40 mL autoclave, sealed, and maintained at 160 °C for 6 h. The resulting product was collected by centrifugation and washed with distilled water and ethanol several times, then dried at 80 °C in air.

Preparation of $NaYF_4$:Yb,Tm/TiO_2 Physical Mixture. $NaYF_4$:Yb,Tm and TiO_2 were synthesized according to the above procedure, and then they were mixed mechanically in the same ratio of $NaYF_4$:Yb,Tm and TiO_2 as that of the $NaYF_4$:Yb,Tm@TiO_2 core−shell composites. The $NaYF_4$:Yb,Tm/TiO_2 ratio in core−shell composites was obtained by elemental analysis ($NaYF_4$:Yb,Tm: TiO_2 = 1:2 in mass, Supporting Information Table S1).

Photocatalytic Experiments. Photocatalysis was performed via monitoring methyl blue (MB) degradation by measuring the optical absorption using a Shimadzu UV-3600 spectrophotometer. In a typical experiment, 0.5 mg of the $NaYF_4$:Yb,Tm@TiO_2 particles was dispersed into a quartz cuvette containing 0.5 mL of MB aqueous solution (15 mg L^{-1}) and then kept in the dark prior to irradiation for establishing adsorption−desorption equilibrium of MB on the surface of $NaYF_4$:Yb,Tm/TiO_2 particles before irradiation. A diode laser of 980 nm with a power of 10 W/cm^2 was used as the irradiation source. After irradiation of 980 nm light for a designated time, 0.3 mL of the MB aqueous solution was taken out for UV−vis absorbance measurements and then put back into the quartz corvette. The concentration of MB solution at each time interval was calculated using the calibration curve of the standard solution. The schematic diagram of the equipment for photocatalytic experiments is shown in Supporting Information Scheme S1.

Detection of Photogenerated OH Radicals. Terephthalic acid (3×10^{-3} M) was dissolved in NaOH (1×10^{-2} M) solution. In a typical process, 15 mg of $NaYF_4$:Yb,Tm@TiO_2 was mixed with 3 mL of terephthalic acid solution, then the mixture was irradiated with a 980 nm NIR laser. Every 30 min, 1.2 mL of the suspensions were collected, and then centrifuged. After that, 1 mL of the solution was diluted four times for the photoluminescence (PL) measurement. The hydroxyterephthalate anion formed was monitored by fluorescence analysis with an excitation wavelength of 320 nm.

Characterization. The purity and phase structure of the resulting products were analyzed with a Rigaku model Ru-200b X-ray powder diffractometer (XRD) using nickel-filtered Cu Ka radiation (λ = 1.5406 Å) in the 2θ range from 20° to 70°. The size and morphology were characterized by using transmission electron microscopy (TEM, JEM 2010F) with an acceleration voltage of 100 kV. Samples for TEM investigations were prepared by first dispersing the particles in ethanol under the assistance of ultrasonification and then dropping one drop of the suspension on a copper TEM grid coated with a holey carbon film. The photoluminescence spectra were recorded at room temperature on a Hitachi F-4500 fluorescence spectrophotometer (1.0 nm for slit width and 400 V for PMT voltage) with excitation of a 980 nm diode laser.

■ RESULTS AND DISCUSSION

Phase and Morphological Characterization. Figure 1a shows the XRD pattern of the as-synthesized upconversion nanocrystal. The position and relative intensity of all diffraction peaks can be readily indexed to the pure cubic $NaYF_4$ according to the JCPDS file NO. 21-1272. No impurity peaks can be identified from the XRD pattern, indicating that the as-synthesized nanophosphors are single-phased. The size and morphology of the as-synthesized upconversion nanophosphors were investigated through TEM. Figure 2a presents a typical TEM image of $NaYF_4$:Yb,Tm nanophosphors that are uniformly distributed in size and dispersed well, and the mean size of these particles is ~25 nm in diameter. Upon the addition of $Ti(OBu)_4$ into the $NaYF_4$:Yb,Tm solution, a titania shell was evidently deposited around the $NaYF_4$:Yb,Tm nanoparticles via the hydrolysis and condensation of $Ti(OBu)_4$, as shown in Figure 2b. The TiO_2 shells are amorphous before

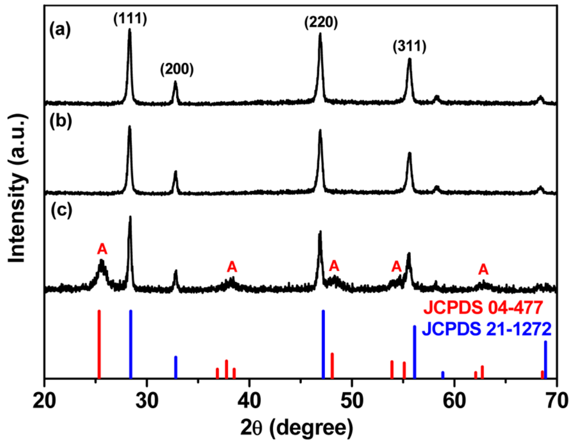

Figure 1. XRD patterns of $NaYF_4$:Yb,Tm nanocrystals with and without titania coating. Standard XRD patterns of JCPDS 21-1272 ($NaYF_4$) and 04-0477 (TiO_2) are also shown. "A" denotes anatase titania.

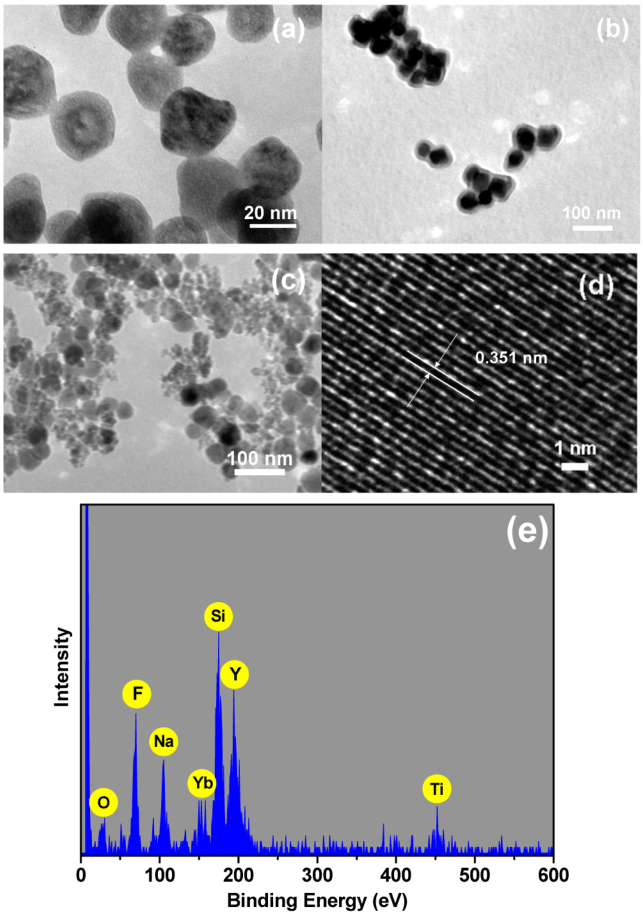

Figure 2. TEM images of $NaYF_4$:Yb,Tm nanocrystals (a), core−shell $NaYF_4$:Yb,Tm@TiO_2 nanoparticles (b) before and (c) after hydrothermal annealing, (d) high-resolution TEM of TiO_2, and (e) EDX spectrum of the $NaYF_4$:Yb,Tm@TiO_2 nanoparticles.

annealing (Figure 1(b). While hydrothermally annealed at 160 °C, the amorphous TiO_2 shells become crystallized. As shown in the XRD pattern of $NaYF_4$:Yb,Tm@TiO_2 (Figure 1c), the characteristic diffraction peaks of TiO_2 can be observed, corresponding to anatase titania according to the JCPDS file NO. 04-0477, while $NaYF_4$ still maintains the cubic structure. Meanwhile, a morphological change also occurred. We can see that the TiO_2 shells are broken to form lots of small-sized nanocrystals around the $NaYF_4$:Yb,Tm particles (Figure 2c) as a result of remarkable shrinkage of the materials and atomic rearrangement due to thermal activation while the size and shape of NaYF4:Yb,Tm particles is almost unchanged. A typical high-resolution TEM image of TiO_2 nanocrystals exhibits a *d*-spacing of 0.351 nm, well-matched to the spacing of (101) of anatase titania (Figure 2d). The EDX spectrum shown in Figure 2e reveals that the samples consist of Y, Yb, Tm, Ti, Na, O, F, and Si. The presence of an Si peak is due to the silicon used as the sample support for the measurement. The photoluminescence characterization of the resulting product provides further evidence of the formation of the $NaYF_4$:Yb,Tm@TiO_2 core−shell structure (see below).

Photoluminescence and Energy Transfer. $NaYF_4$:Yb^{3+},Tm^{3+} is a typical upconversion (UC) luminescence material for NIR-to-UV light. In essence, upconversion is a multiphoton process in which the NIR excitation light (typically 980 nm) is converted to higher energies from the deep UV to the NIR via successive energy transfer processes.[41−43] Under a 980 nm laser excitation, $NaYF_4$ codoped with Yb and Tm ions emits UV and blue light, as shown in Figure 3. UV emission peaks centered at 291, 349, and 362 nm are attributed to the transitions of Tm ions: $^1I_6 \rightarrow {}^3H_6$, $^1I_6 \rightarrow {}^3F_4$, and $^1D_2 \rightarrow {}^3H_6$, respectively. Two blue emission peaks centered at 450 and 474 nm are assigned to $^1D_2 \rightarrow {}^3F_4$ and $^1G_4 \rightarrow {}^3H_6$ transitions of Tm^{3+} ions, respectively. It is worth mentioning that strong UV light is obtained in $NaYF_4$:Yb,Tm upon NIR excitation, which is especially useful to realize the NIR-driven photocatalytic activity of $NaYF_4$:Yb,Tm@TiO_2 that will be investigated in the following section.

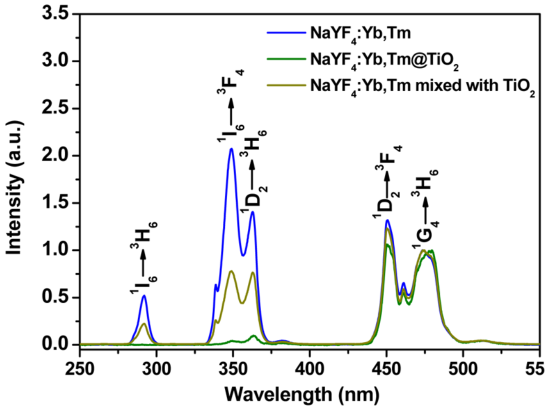

Figure 3. PL spectra of $NaYF_4$:Yb,Tm, $NaYF_4$:Yb,Tm/TiO_2 core−shell composite, and $NaYF_4$:Yb,Tm/TiO_2 physical mixture under 980 nm excitation at room temperature.

After coating $NaYF_4$:Yb,Tm nanoparticles with titania, notable spectral differences can be observed (Figure 3). The emission peak at 291 nm nearly disappears, and the emission intensities of ∼347 nm and ∼362 nm decrease significantly in comparison with the UC fluorescence spectra of $NaYF_4$:Yb,Tm nanocrystals, whereas those centered at 452 and 474 nm remain almost unchanged, indicating that the spectral change should be relevant to the presence of the titania nanoparticles around upconversion $NaYF_4$:Yb,Tm particles.

To ascertain the origin of photoluminescence spectral changes, UV−vis−NIR absorption spectra of $NaYF_4$:Yb,Tm nanocrystals coated and uncoated with titania were measured, as shown in Figure 4. On the observation of the absorbance spectra of the sample coated with TiO_2, a sharp peak starting at 400 nm emerged, corresponding to its bandgap absorption of ~3.2 eV (~380 nm). Therefore, we can speculate that the UV photon energy generated via the upconversion process of $NaYF_4$:Yb,Tm has been absorbed by the anatase TiO_2 around $NaYF_4$:Yb,Tm particles via an energy transfer between them.

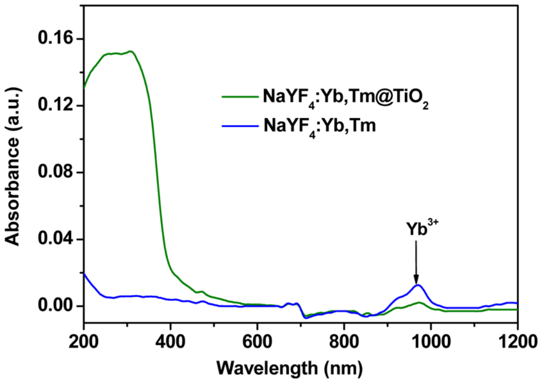

Figure 4. UV−vis−NIR absorbance spectra of $NaYF_4$:Yb,Tm nanocrystals with and without titania coating.

Such a conclusion was further supported by time-resolved fluorescence dynamic curves of Tm^{3+}. The fluorescence dynamic curves of $^1I_6$ (349 nm), $^1D_2$ (450 nm), and $^1G_4$ (474 nm) levels of Tm^{3+} ions in $NaYF_4$:Yb,Tm coated with and without TiO_2 were recorded at the excitation wavelength of 953.6 nm, as shown in Figure 5. The average decay times of $^1I_6$ and $^1D_2$ levels decreased significantly after TiO_2 coating, but that of the $^1G_4$ level changed little. This suggests that the $^1I_6$ and $^1D_2$ levels of Tm^{3+} in $NaYF_4$ match well with the bandgap of anatase TiO_2. As we know, the lifetime of an excited state, τ, is determined by the radiative transition rate (W_R), the nonradiative transition rate (W_{NR}), and the energy transfer rate (W_{ET}), which can be expressed as $\tau = 1/(W_R + W_{NR} + W_{ET})$.[44,45]

The presence of anatase TiO_2 around $NaYF_4$:Yb,Tm particles creates nonradiative energy transfer channels from the excited states of Tm^{3+} ions to TiO_2. Such an additional energy transfer process obviously accelerates the relaxation of the excited states of Tm^{3+}, that is, the increase in the overall transition rates and, thus, the reduction of the fluorescence lifetime. The shortening of the fluorescence lifetime of Tm^{3+} after TiO_2 coating indicates the energy migration between $NaYF_4$:Yb,Tm and TiO_2 is a fluorescence resonance energy transfer (FRET) process, rather than a radiation−reabsorption process, because the fluorescence lifetime of the donor is unchanged in the latter process. Therefore, the energy of the excited state $^1I_6$ and $^1D_2$ of Tm^{3+} is transferred directly to semiconductor TiO_2, since these two excited state levels match with the bandgap of TiO_2. The understanding of the energy transfer process and pathway between $NaYF_4$:Yb,Tm and TiO_2, is very important because the energy migration to TiO_2 is a prerequisite to realize NIR-responsive photocatalysis of broadband TiO_2.

To further demonstrate the importance of the energy migration process, we also measured the photoluminescence of the physical mixtures of $NaYF_4$:Yb,Tm and TiO_2. The intensities of the UV emissions decreased (Figure 3), compared with those from pure $NaYF_4$:Yb,Tm, but the lifetimes of the corresponding excited states changed a little (Figure 5), which indicated that the UV emissions were reduced mainlyby radiation−reabsorption processes in the mixture. These two different energy migration processes lead to the difference in the energy transfer efficiencies. The energy transfer efficiency in the $NaYF_4$:Yb,Tm/TiO_2 core−shell composite is higher than that in the physical mixture of $NaYF_4$:Yb,Tm/TiO_2, which is indicated clearly by the emission spectra shown in Figure 3. Especially, it is worth emphasizing that the difference in the

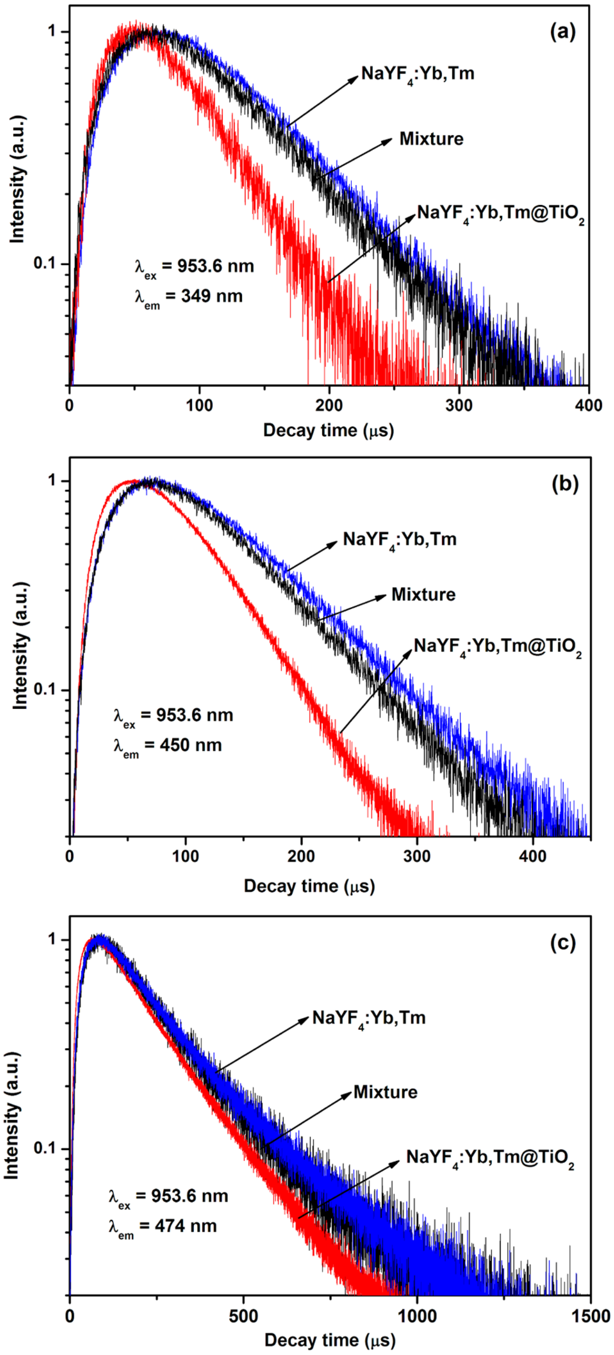

Figure 5. Luminescence dynamic curves of the (a) $^1I_6$ level, (b) $^1D_2$ level, and (c) $^1G_4$ level of Tm^{3+} in $NaYF_4$:Yb,Tm, $NaYF_4$:Yb,Tm/TiO_2 core−shell composite and $NaYF_4$:Yb,Tm/TiO_2 physical mixture at the excitation wavelength of 953.6 nm.

energy transfer routes from Tm^{3+} to TiO_2 affects the photocatalytic activity of TiO_2 markedly, which will be discussed in the Photocatalytic Activity section below.

Photocatalytic Activity. MB was used as a model pollutant to investigate the photocatalytic activity of $NaYF_4$:Yb,Tm@TiO_2 hybrid materials under NIR irradiation of 980 nm. A 0.5 mg portion of the $NaYF_4$:Yb,Tm@TiO_2 particles was dispersed into a quartz cuvette containing 0.5 mL of MB aqueous solution (15 mg L^{-1}). For obtaining the real concentration of MB decomposed by photocatalysis, the dark reaction of MB in the presence of catalysts was conducted to establish the adsorption/desorption equilibrium of MB on the surfaces of the $NaYF_4$:Yb,Tm/TiO_2 particles. Upon NIR irradiation for a designated time, 0.4 mL of MB aqueous solution was taken out for absorbance measurement.

Figure 6a shows the absorbance spectra of MB catalyzed by the $NaYF_4$:Yb,Tm@TiO_2 nanoparticles under NIR irradiation as a function of the irradiation time. The absorption intensity of MB at 664 nm decreases gradually with the increase in the irradiation time, indicating the degradation of MB upon the NIR irradiation. The photocatalytic activity of $NaYF_4$:Yb,Tm@TiO_2 can be evaluated through the concentration of MB after NIR irradiation relative to original one of MB. Figure 6b shows the time-dependent ratios of C/C_0, where C_0 is the original concentration of MB and C is the concentration of MB irradiated with a 980 nm laser for time t or nonirradiated for time t in the dark reaction. C can be calibrated by comparing the absorption of the MB solution with that of the standard MB solution at a wavelength of 664 nm. Thus, the value of C/C_0 stands for the degradation degree of MB. We can see that a very small concentration of MB was adsorbed at the particles' surfaces in the aqueous solution in the dark reaction so that these adsorptions were almost negligible for the calculation of the degradation ratio in the photocatalytic reactions. From Figure 6b, the degradation ratio of MB was shown to increase continuously with the irradiation time and reached about 65% after 14 h irradiation in the presence of $NaYF_4$:Yb,Tm@TiO_2 particles.

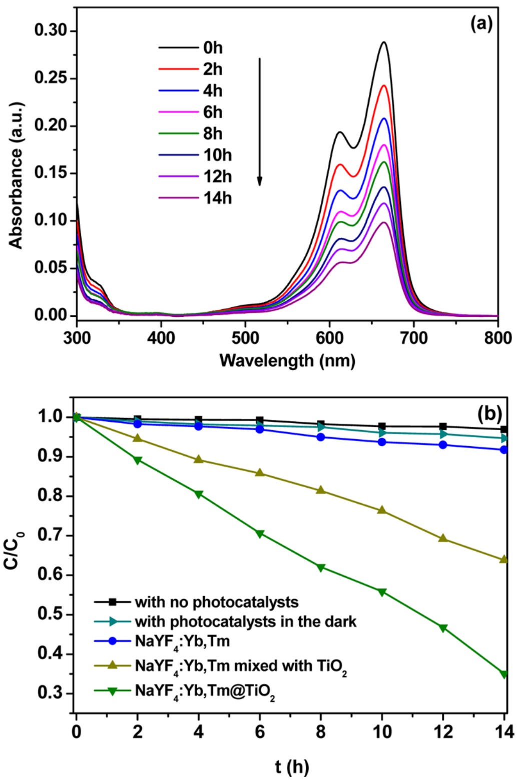

Figure 6. (a) Absorbance spectra of MB catalyzed by the core−shell photocatalyst at different irradiation times under NIR excitation; (b) the time-dependent ratios of C/C_0 in the presence of $NaYF_4$:Yb,Tm, $NaYF_4$:Yb,Tm/TiO_2 core−shell composite and $NaYF_4$:Yb,Tm/TiO_2 physical mixture, and with photocatalysts in the dark, respectively.

To demonstrate the origin of MB degradation upon NIR irradiation in the presence of $NaYF_4$:Yb,Tm@TiO_2 particles, a series of parallel experiments were performed as follows: (i) MB solution was irradiated with NIR light in the absence of $NaYF_4$:Yb,Tm and TiO_2. In this case, almost no degradation of MB occurred. (ii) MB solution was irradiated with NIR light in the presence of $NaYF_4$:Yb,Tm, and only ∼8% of MB was decomposed. As we know, both NIR irradiation and nonradiative relaxations of excited Yb^{3+} and Tm^{3+} ions can generate thermal energy. The temperature of the MB solution was recorded with time upon 980 nm irradiation in the presence of upconverting $NaYF_4$:Yb,Tm (Figure S1, Supporting Information). We can see that the temperature increased with time and reached 38 °C from the original 7 °C after 1 h of irradiation, and then it was maintained at this temperature (the experiments were carried out in Changchun, China in winter). The results in the above two control experiments indicate that the thermal energy generated by NIR irradiation is not enough to induce thermal degradation of MB significantly. Furthermore, to verify whether such a temperature increase with irradiation time contributes to the photocatalysis to a certain extent, we conducted the comparative experiments: (1) photocatalysis in a constant temperature by adding an ice/water mixture in the photocatalytic equipment and (2) photocatalysis in a varying temperature (changed from 7 to 38 °C at the initial 1 h and then maintained at 38 °C). We found that such a varying temperature did not contribute to the photocatalysis significantly, since almost the same degradation ratio was obtained for experiments 1 and 2.

For comparing the difference in the photocatalytic properties for $NaYF_4$:Yb,Tm@TiO_2 nanoparticles and the $NaYF_4$:Yb,Tm/TiO_2 mixture, the MB solution was irradiated with NIR light in the presence of the $NaYF_4$:Yb,Tm/TiO_2 mixture, and 30% of the MB was found to be decomposed, which is two times lower than the case of $NaYF_4$:Yb,Tm/TiO_2 core−shell particles (∼65%). This could be attributed to the difference in their energy migration routes, as has been discussed in the Photoluminescence section. In the core−shell structured particles, $NaYF_4$:Yb,Tm and TiO_2 attach closely to each other and form compact interfaces, which benefits FRET processes. In contrast, there are no contact interfaces between $NaYF_4$:Yb,Tm and TiO_2 particles in the physical mixture, and thus, TiO_2 can be excited mainly via radiation−reabsorption. Therefore, in the core−shell-structured $NaYF_4$:Yb,Tm@TiO_2, more NIR photon energy has been used to activate TiO_2 and induces a relatively high photocatalytic activity. These results indicate that FRET is an important mechanism in the NIR photocatalytic activity.

Generally, the reactive oxygen species produced in the photocatalytic reaction, especially hydroxyl radicals (·OH), were considered responsible for the degradation of pollutant molecules because of their strong oxidation ability. To verify the production of ·OH during the photocatalytic process of $NaYF_4$:Yb,Tm@TiO_2 particles under NIR irradiation, we used a fluorescence probe with terephthalic acid (TA) for the measurement of ·OH generation.[46] It is known that TA itself does not emit fluoresce.[47] The nonfluorescent TA captures ·OH to generate hydroxyterephthalic acid (TAOH), which emits fluorescence at ~426 nm on the excitation of 320 nm UV light.[47] Therefore, the formation of TAOH as well as the generation of ·OH can be selectively and quantifiably detected by monitoring the emission intensity at 426 nm.

Figure 7a shows photoluminescence spectra for the supernatant solution of the photocatalyst suspension containing 3 mM TA irradiated with NIR for various times. The recorded spectra are characteristic of the fluorescence of TAOH, which indicates that ·OH has been produced during the NIR photocatalytic reactions. Figure 7b presents the integration of the emission of TAOH as a function of irradiation time. The generation rate of ·OH can be evaluated by the slopes of the curves in Figure 7b. The larger the slope is, the faster ·OH generates. Combining Figure 6a with Figure 7a, we also find that the photocatalytic activity increases with an increase in the ·OH generation rate. From Figure 7b, we can see that, upon NIR irradiation, almost no ·OH was generated in the case of no catalyst or with $NaYF_4$:Yb,Tm; thus, almost no degradation of organic species occurred in the two cases. On the other hand, in the presences of the core−shell $NaYF_4$:Yb,Tm@TiO_2 or $NaYF_4$:Yb,Tm/TiO_2 physical mixture, ·OH was produced upon NIR irradiation. Moreover, the presence of core−shell $NaYF_4$:Yb,Tm@TiO_2 generated more ·OH than that of the $NaYF_4$:Yb,Tm/TiO_2 physical mixture. As a result, a higher photocatalytic activity can be achieved for the former than the latter. This is still attributed to the fact that the FRET is efficient in core−shell $NaYF_4$:Yb,Tm@TiO_2. In this way, more NIR photon energy can be used to activate TiO_2 and produce more electron−hole pairs for photocatalysis. These results indicate that the energy transfer efficiency between $NaYF_4$:Yb,Tm and TiO_2 is the key to affect the NIR photocatalytic activity. In addition, it should be noted that the relationship between the ·OH generation rate and the photocatalytic activity implies that the NIR photocatalytic activity arises from ·OH.

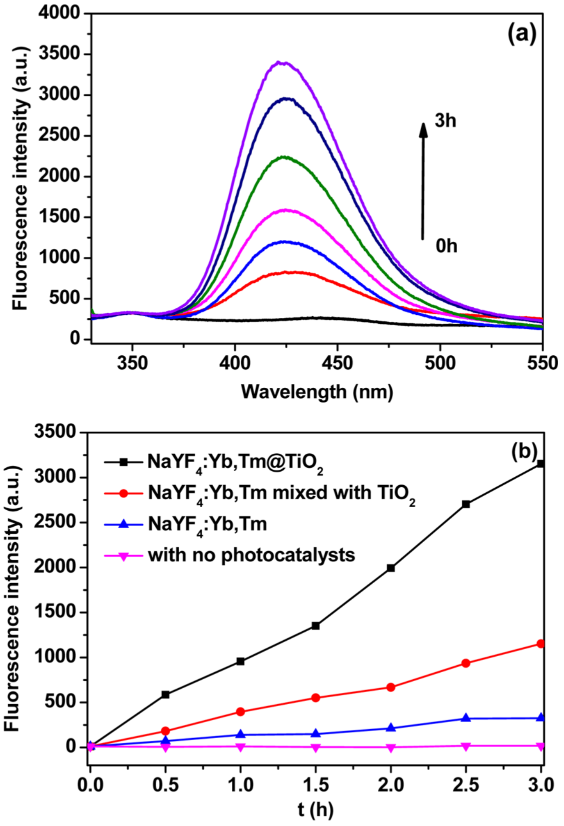

Figure 7. (a) Time-dependent fluorescence spectra of the terephthalic acid solution containing 15 mg of $NaYF_4$:Yb,Tm/TiO_2 core−shell composite upon NIR irradiation and (b) the integration of the emission of TAOH as a function of NIR irradiation time in the presence of $NaYF_4$:Yb,Tm, $NaYF_4$:Yb,Tm/TiO_2 core−shell composite, and $NaYF_4$:Yb,Tm/TiO_2 physical mixture, respectively.

Mechanism. Scheme 1 illustrates the diagrams of energy levels of Yb^{3+}−Tm^{3+} and upconversion luminescence processes in an Yb^{3+}−Tm^{3+} codoped system upon 980 nm excitation. The pump light of 980 nm excites only the Yb^{3+} ions, and three successive energy transfers from Yb^{3+} to Tm^{3+} populate the $^3H_5$, $^3F_2$, and $^1G_4$ levels.[48] The $^1D_2$ level of Tm^{3+} cannot be populated directly by the fourth photon from Yb^{3+} via energy transfer to the $^1G_4$ because of the large energy mismatch (about 3500 cm^{-1}) between them.[49] The cross-relaxation between Tm^{3+} ions may be responsible for populating the $^1D_2$ level. Usually, there are primarily two cross-relaxation processes in populating the $^1D_2$ level: $^3F_2 + {}^3H_4 \rightarrow {}^3H_6 + {}^1D_2$, and $^1G_4 + {}^3H_4 \rightarrow {}^3F_4 + {}^1D_2$.[48,50,51] On the other hand, the $^1D_2$ state may be promoted to the $^3P_2$ state via another energy transfer from excited Yb^{3+} and then relaxed nonradiatively to the $^1I_6$ level (Scheme 1).

Scheme 1. Diagrams of Energy Levels of Yb^{3+}-Tm^{3+} and Upconversion Luminescence Processes in an Yb^{3+}−Tm^{3+} Codoped System upon 980 nm Excitation

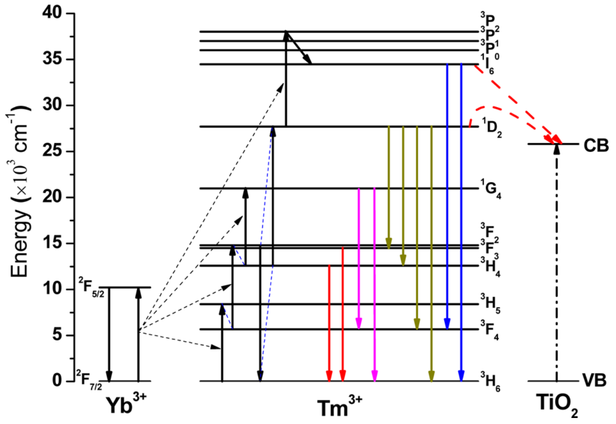

As discussed earlier, the n-type anatase semiconductor TiO_2 is excited mainly by the energy transfer from $^1D_2$ and $^1I_6$ levels of Tm^{3+} ions via FRET processes. Thus, TiO_2 is activated to produce electrons and holes in the conduction band (CB) and the valence band (VB) (see Scheme 2), and then these electron−hole pairs migrate from the inner region to the surfaces to take part in surface reactions.

As shown in Scheme 2, the excited electrons arriving on the surfaces react with the oxygen adsorbed on the surfaces of TiO_2 to form O^{2-} or $O_2{}^{2-}$, which combines with H^+ to form hydrogen peroxide (H_2O_2).[52] H_2O_2 can react with the superoxide radical anion ($O_2 \cdot^-$), reducing to hydroxyl radicals (·OH),[52] whereas the photogenerated holes can react with H_2O to form hydroxyl radicals (·OH).[52,53] The oxidized form of MB is oxidized methylene blue ($MB^{\bullet+}$).[54] The conduction band of TiO_2 is located above the MB redox potential ($E^0_{MB\bullet+/MB}$ =

Scheme 2. Illustrative Diagrams of Energy Transfer among Yb^{3+}, Tm^{3+}, and TiO_2; the Generation of OH Radicals via the Reaction of Electron and Hole with the Surface Species of TiO_2; and the Energy Scales

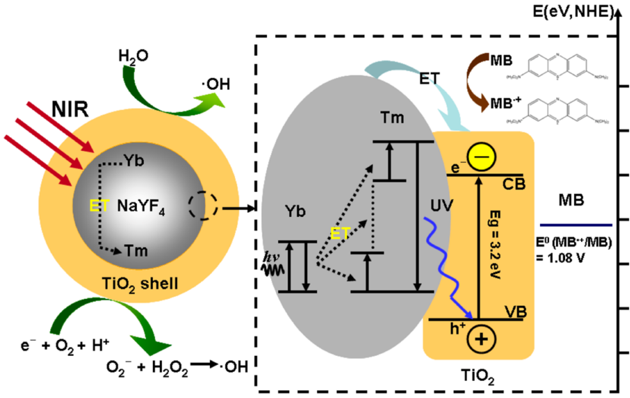

1.08 V versus normal hydrogen electrode (NHE)), allowing TiO_2 to be catalytically active.[54,55] Therefore, these reactive oxygen species (e.g., ·OH, $O_2{\cdot}^-$, and H_2O_2), especially ·OH, can oxidize the organic molecules and perform photocatalysis.[52,53,56−58]

CONCLUSIONS

Upconversion luminescence nanoparticles $NaYF_4$:Yb,Tm were prepared by a solvothermal process, and TiO_2 nanocrystals were deposited on the $NaYF_4$:Yb,Tm particles via a method similar to a Stöber process based on the hydrolysis and condensation of $Ti(OBu)_4$. XRD, TEM, EDX, and spectral analysis revealed that anatase titania nanocrystals were attached around cubic $NaYF_4$:Yb,Tm particles, forming $NaYF_4$:Yb,Tm@TiO_2 core−shell nanostructures. The degradation of MB exposed to $NaYF_4$:Yb,Tm@TiO_2 core−shell particles upon NIR radiation demonstrated the NIR-driven photocatalytic capability. For comparison, the physical mixture of $NaYF_4$:Yb,Tm and TiO_2 was prepared by mixing individual $NaYF_4$:Yb,Tm and TiO_2 powders mechanically. Steady-state and dynamic fluorescent analysis revealed that the energy transfer routes are different for $NaYF_4$:Yb,Tm@TiO_2 core−shell composites and the mixtures of $NaYF_4$:Yb,Tm and TiO_2. FRET and radiation−reabsorption mechanisms are confirmed to dominate in NIR photocatalysis for the two different photocatalysts, respectively. Furthermore, FRET is efficient, so more energy can be transferred from the excited states of Tm^{3+} ions to TiO_2. Therefore, the $NaYF_4$:Yb,Tm@TiO_2 core−shell composites have higher photocatalytic activity than the mixture of $NaYF_4$:Yb,Tm and TiO_2. A fluorescence probe with terephthalic acid (TA) was used to monitor the generation of OH radicals and revealed the mechanism of NIR-driven photocatalytic degradation of organic compounds.

ASSOCIATED CONTENT

Ⓢ Supporting Information

The scheme for the photocatalytic reaction equipment; the elemental analysis of $NaYF_4$:Yb,Tm@TiO_2 core−shell nanoparticles; the temperature versus 980 nm irradiation time. This information is available free of charge via the Internet at http://pubs.acs.org/.

AUTHOR INFORMATION

Corresponding Author

*Address: 2699 Qianjin Street, Changchun 130012, China. Phone: 86-431-85168240-8325. Fax: 86-431-85168240-8325. E-mail: whdi@jlu.edu.cn (W.D.), wpqin@jlu.edu.cn (W.Q.)

Notes

The authors declare no competing financial interest.

ACKNOWLEDGMENTS

This work was supported by the NSFC (Grants Nos. 61178073, 51072065, 60908031, 60908001, and 61077033), the Program for NCET in University (No: NCET-08-0243), the Opened Fund of the State Key Laboratory on Integrated Optoelectronics, and Tsinghua National Laboratory for Information Science and Technology (TNList) Cross-discipline Foundation.

REFERENCES

(1) Fujishima, A.; Honda, K. *Nature* **1972**, *238*, 37−38.
(2) Hoffmann, M. R.; Martin, S. T.; Choi, W.; Bahnemann, D. W. *Chem. Rev.* **1995**, *95*, 69−96.
(3) Linsebigler, A. L.; Lu, G.; Yates, J. T., Jr. *Chem. Rev.* **1995**, *95*, 735−758.
(4) Fox, M. A.; Dulay, M. T. *Chem. Rev.* **1993**, *93*, 341−357.
(5) Chen, X.; Mao, S. S. *Chem. Rev.* **2007**, *107*, 2891−2959.
(6) O'Regan, B.; Grätzel, M. *Nature* **1991**, *353*, 737−740.
(7) Grätzel, M. *Nature* **2001**, *414*, 338−344.
(8) Aita, H.; Hori, N.; Takeuchi, M.; Suzuki, T.; Yamada, M. *Biomaterials* **2009**, *30*, 1015−1025.
(9) Furukawa, S.; Shishido, T.; Teramura, K.; Tanaka, T. *ACS Catal.* **2012**, *2*, 175−179.
(10) Tsukamoto, D.; Shiro, A.; Shiraishi, Y.; Sugano, Y.; Ichikawa, S.; Tanaka, S.; Hirai, T. *ACS Catal.* **2012**, *2*, 559−603.
(11) Zhu, Q.; Qian, J. S.; Pan, H.; Tu, L.; Zhou, X. F. *Nanotechnology* **2011**, *22*, 395703.
(12) Rozhkova, E. A.; Ulasov, I.; Lai, B.; Dimitrijevic, N. M.; Lesniak, M. S.; Rajh, T. *Nano Lett.* **2009**, *9*, 3337−3342.
(13) Asahi, R.; Taga, Y.; Mannstadt, W.; Freeman, A. J. *Phys. Rev. B* **2000**, *61*, 7459−7465.
(14) Amtout, A.; Leonelli, R. *Phys. Rev. B* **1995**, *51*, 6842−6851.
(15) Koelsch, M.; Cassaignon, S.; Thanh Minh, C. T.; Guillemoles, J.-F.; Jolivet, J.-P. *Thin Solid Films* **2004**, *451*, 86−92.
(16) Qin, W. P.; Zhang, D. S.; Zhao, D.; Wang, L. L.; Zheng, K. Z. *Chem. Commun.* **2010**, *46*, 2304−2306.
(17) Asahi, R.; Morikawa, T.; Ohwaki, T.; Aoki, K.; Taga, Y. *Science* **2001**, *293*, 269−271.
(18) Izumi, Y.; Itoi, T.; Peng, S.; Oka, K.; Shibata, Y. *J. Phys. Chem. C* **2009**, *113*, 6706−6718.
(19) Zhang, J.; Wu, Y.; Xing, M.; Leghari, S. A. K.; Sajjad, S. *Energy Environ. Sci.* **2010**, *3*, 715−726.
(20) Huang, G. L.; Zhu, Y. F. *J. Phys. Chem. C* **2007**, *111*, 11952−11958.
(21) Chen, S. H.; Sun, S. X.; Sun, H. G.; Fan, W. L.; Zhao, X.; Sun, X. *J. Phys. Chem. C* **2010**, *114*, 7680−7688.
(22) Murakami, N.; Chiyoya, T.; Tsubota, T.; Ohno, T. *Appl. Catal., A* **2008**, *348*, 148−152.
(23) Murakami, N.; Ono, A.; Nakamura, M.; Tsubota, T.; Ohno, T. *Appl. Catal., B* **2010**, *97*, 115−119.
(24) Behar, D.; Rabani, J. *J. Phys. Chem. B* **2006**, *110*, 8750−8755.
(25) Zeng, Y.; Wu, W.; Lee, S.; Gao. *J. Catal. Commun.* **2007**, *8*, 906−912.
(26) Wang, W.; Zhang, J.; Chen, F.; He, D.; Anpo, M. *J. Colloid Interface Sci.* **2008**, *323*, 182−186.
(27) Pelaez, M.; Nolan, N. T.; Pillai, S. C.; Seery, M. K.; Falaras, P.; Kontos, A. G.; Dunlop, P. S. M; Hamilton, J. W. J.; Byrne, J. A.; O'Shea, K.; Entezari, M. H.; Dionysiou, D. D. *Appl. Catal., B* **2012**, *125*, 331−349.

(28) Choi, W.; Termin, A.; Hoffmann, M. R. *J. Phys. Chem.* **1994**, *98*, 13669−13679.

(29) Xu, L.; Steinmiller, E. M. P.; Skrabalak, S. E. *J. Phys. Chem. C* **2012**, *116*, 871−877.

(30) Chuang, H.; Chen, D. H. *Nanotechnology* **2009**, *20*, 105704.

(31) Liu, H. R.; Shao, G. X.; Zhao, J. F.; Zhang, Z. X.; Zhang, Y.; Liang, J.; Liu, X. G.; Jia, H. S.; Xu, B. S. *J. Phys. Chem. C* **2012**, *116*, 16182−16190.

(32) Neelgund, G. M.; Oki, A. *Appl. Catal., B* **2011**, *110*, 99−107.

(33) Fouad, D.; Mamdouh, M.; Mona, B. *Nanotechnology* **2011**, *22*, 455705.

(34) Zhang, N.; Liu, S. Q.; Xu, Y. J. *Nanoscale* **2012**, *4*, 2227−2238.

(35) Liang, Q. H.; Shi, Y.; Ma, W. J.; Li, Z.; Yang, X. M. *Phys. Chem. Chem. Phys.* **2012**, *14*, 15657−15665.

(36) Zhang, P.; Shao, C. L.; Zhang, Z. Y.; Zhang, M. Y.; Mu, J. B.; Guo, Z. C.; Liu, Y. C. *Nanoscale* **2012**, *3*, 2943−2949.

(37) Di, W. H.; Velu, S. K. P.; Lascialfari, A.; Chunxu Liu, C. X.; Pinna, N.; Arosio, P.; Sakka, Y.; Qin, W. P. *J. Mater. Chem.* **2012**, *22*, 20641−20648.

(38) Dong, B. A.; Xu, S.; Sun, J. A.; Bi, S.; Li, D.; Bai, X.; Wang, Y.; Wang, L. P.; Song, H. W. *J. Mater. Chem.* **2011**, *21*, 6193−6200.

(39) Demirörs, A. F.; van Blaaderen, A.; Imhof, A. *Langmuir* **2010**, *26*, 9297−9303.

(40) Golubko, N. V.; Yanovskaya, M. I.; Romm, I. P. *J. Sol-Gel Sci. Technol.* **2001**, *20*, 245−262.

(41) Jiang, T.; Qin, W. P.; Di, W. H.; Yang, R. Y.; Liu, D. M.; Zhai, X. S.; Qin, G. S. *Crystengcomm* **2012**, *14*, 2302−2307.

(42) Liu, Y. S.; Tu, D. T.; Zhu, H. M.; Li, R. F.; Luo, W. Q.; Chen, X. Y. *Adv. Mater.* **2010**, *22*, 3266−3271.

(43) Ren, W. L.; Tian, G.; Jian, S.; Gu, Z. j.; Zhou, L. J.; Yan, L.; Jin, S.; Yin, W. Y.; Zhao, Y. L. *RSC Adv.* **2012**, *2*, 7037−7041.

(44) Di, W. H.; Wang, X. J.; Chen, B. J.; Lu, S. Z.; Zhao, X. X. *J. Phys. Chem. B* **2005**, *109*, 13154−13158.

(45) Yu, L. X.; Song, H. W.; Liu, Z. X.; Yang, L. M.; Lv, S. Z.; Zheng, Z. H. *J. Phys. Chem. B* **2005**, *119*, 11450−5.

(46) Ishibashi, K.; Fujishima, A.; Watanabe, T.; Hashimoto, K. *J. Photochem. Photobiol. A* **2000**, *134*, 139−142.

(47) Armstrong, W. A.; Facey, R. A.; Grant, D. W.; Humpherys, W. G. *Can. J. Chem.* **1963**, *41*, 1575−1577.

(48) Chen, X. B.; Song, Z. F. *J. Opt. Soc. Am. B* **2006**, *24*, 965−971.

(49) Qin, G. S.; Qin, W. P.; Wu, C. F.; Huang, S. H.; Zhang, J. S.; Lu, S. Z.; Zhao, D.; Liu, H. Q. *J. Appl. Phys.* **2003**, *99*, 1−3.

(50) Wang, G. F.; Qin, W. P.; Wang, L. L.; Wei, G. D.; Zhu, P. F.; Kim, R. J. *Opt. Express* **2008**, *16*, 11907−11904.

(51) Chen, D. Q.; Wang, Y. S.; Yu, Y. L.; Huang, P. *Appl. Phys. Lett.* **2007**, *91*, 051920−051922.

(52) Kang, Q.; Lu, Q. Z.; Liu, S. H.; Yang, L. X.; Wen, L. F.; Luo, S. L.; Cai, Q. Y. *Biomaterials* **2010**, *31*, 3317−3326.

(53) Sarkar, A.; Shchukarev, A.; Leino, A.; Kordas, K.; Mikkola, J.; Petrov, P.; Tuchina, E.; Popov, A.; Darvin, M.; Meinke, M.; Lademann, J.; Tuchin, V. *Nanotechnology* **2012**, *23*, 475711.

(54) Mills, A.; Wang, J. S. *J. Photochem. Photobiol. A: Chem.* **1999**, *127*, 123−134.

(55) Vilar-Vidal, N.; Rivas, J.; Lopez-Quintela, M. A. *ACS Catal.* **2012**, *2*, 1693−1697.

(56) Houas, A.; Lachheb, H.; Ksibi, M.; Elaloui, E.; Guillard, C.; Hermann, J. M. *Appl. Catal. B: Environ.* **2001**, *31*, 145−157.

(57) Wang, X. D.; Dornom, T.; Blackford, M.; Caruso, R. A. *J. Mater. Chem.* **2012**, *22*, 11701−11710.

(58) Vijayan, B. K.; Dimitrijevic, N. M.; Finkelstein-Shapiro, D.; Wu, J. S.; Gray, K. A. *ACS Catal.* **2012**, *2*, 223−229.